POLITECNICO DI TORINO
Repository ISTITUZIONALE

Enhancing surface heat transfer by carbon nanofins: towards an alternative to nanofluids?

(Article begins on next page)

25 April 2024

Enhancing surface heat transfer by carbon nanofins: Towards an alternative to nanofluids?

Eliodoro Chiavazzo[1], Pietro Asinari[1,*]

[1]Department of Energetics, Politecnico di Torino, Corso Duca degli Abruzzi, 10129 Torino, Italy

Email: Eliodoro Chiavazzo - eliodoro.chiavazzo@polito.it; Pietro Asinari*- pietro.asinari@polito.it;

*Corresponding author

Abstract

Background: Nanofluids are suspensions of nanoparticles and fibers which have recently attracted much attention due to their superior thermal properties. Nevertheless, it was proven that, due to modest dispersion of nanoparticles, such high expectations often remain unmet. Here, by introducing the notion of *nanofin* a possible solution is envisioned, where nanostructures with high aspect-ratio are sparsely attached to a solid surface (in order to avoid a significant disturbance on the fluid dynamic structures), and act as efficient thermal bridges within the boundary layer. As a result, particles are only needed in a small region of the fluid, while dispersion can be controlled in advance by design and manufacturing processes.

Results: Toward the end of implementing the above idea, we focus on single carbon nanotubes to enhance heat transfer between a surface and a fluid in contact with it. First, we investigate the thermal conductivity of the latter nanostructures by means of classical non-equilibrium molecular dynamics simulations. Next, thermal conductance at the interface between a single wall carbon nanotube (nanofin) and water molecules is assessed by means of both steady-state and transient numerical experiments.

Conclusions: Numerical evidences suggest a pretty favorable thermal boundary conductance (order of 10^7 $[Wm^{-2}K^{-1}]$) which makes carbon nanotubes potential candidates for constructing *nanofinned surfaces*.

Background and motivations

Nanofluids are suspensions of solid particles and/or fibers, which have recently become a subject of growing scientific interest because of reports of greatly enhanced thermal properties [1, 2]. Filler dispersed in a nanofluid is typically of nanometer size, and it has been shown that such nanoparticles are able to endow a base fluid with a much higher effective thermal conductivity than fluid alone [3, 4]: Significantly higher than those of commercial coolants such as water and ethylene glycol. In addition, nanofluids show an enhanced thermal conductivity compared to theoretical predictions based on the Maxwell equation for a well-dispersed particulate composite model. These features are highly desirable for applications, and nanofluids may be a strong candidate for new generation of coolants [2]. A review about experimental and theoretical results on the mechanism of heat transfer in nanofluids can be found in Ref. [5], where Authors discuss issues related to the technology of nanofluid production, experimental equipment, and features of measurement methods. A large degree of randomness and scatter has been observed in the experimental data published in the open literature. Given the *inconsistency* in these data, it is impossible to develop a comprehensive physical-based model that can predict all the experimental evidences. This also points out the need for a systematic approach in both experimental and theoretical studies [6].

In particular, carbon nanotubes (CNTs) have attracted great interest for nanofluid applications, because of the claims about their exceptionally high thermal conductivity [7]. However, recent experimental findings about CNTs report an *anomalously* wide range of enhancement values that continue to perplex the research community and remain unexplained [8]. For example, some experimental studies showed that there is a modest improvement in thermal conductivity of water at a high loading of multi-walled carbon nanotubes (MW-CNTs), $\sim$35% increase for a 1 wt% MWNT nanofluid [9]. These authors attribute the increase to the formation of a nanotube network with a higher thermal conductivity. On the contrary, at low nanotube content, <0.03 wt%, they observed a decrease in thermal conductivity upon an increase of nanotube concentration. On the other hand, more recent experimental investigations showed that the enhancement of thermal conductivity as compared to water is varying linearly when MW-CNT weight content is increasing from 0.01 to 3 wt%. For a MWNT weight content of 3 wt% the enhancement of thermal conductivity reaches 64% of the base fluid (e.g. water). The average length of the nanotubes appears to be a very sensitive parameter. The enhancement of thermal conductivity compared to water alone is enhanced when nanotube average length is increasing in the 0.5-5 μm range [10].

Clearly, there are difficulties in the experimental measurements [11], but the previous results also reveal some underlaying technological problems. First of all, the CNTs show some bundling or the formation of aggregates originating from the fabrication step. Moreover it seems reasonable that CNTs encounter *poor dispersibility* and suspension durability due to the aggregation and surface hydrophobicity of CNTs as a nanofluid filler. Therefore, the surface modification of CNTs or additional chemicals (surfactants) have been required for stable suspensions of CNTs, due to the polar characteristics of base fluid. In the case of surface modification of CNTs, water-dispersible CNTs have been extensively investigated for potential applications, such as biological uses, nanodevices, novel precursors for chemical reagents, and nanofluids [2]. From the above brief review, it is possible to conclude that, despite the great interest and intense research in this field, the results achieved so far cannot be considered really encouraging. Here, toward the end of overcoming these problems, we introduce the notion of *thermal nanofins*, with an entirely different meaning with respect to standard terminology. By nanofins, we mean slender nano-structures, sparse enough in order not to interfere with the thermal boundary layer, but sufficiently rigid and conductive to allow direct energy transfer between the wall and the bulk fluid, thus acting as thermal bridges. A macroscopic analogy is given by an eolic park, where wind towers are slim enough to avoid disturbing the planetary boundary layer, but high enough to reach the region where wind is stronger (see Fig. 3.2). In this way, nanoparticles are used only where they are needed, namely in the thermal boundary layer (or in the thermal laminar sub-layer, in case of turbulent flows, not discussed here), and this might finally unlock the enormous potential of the basic idea behind nanofluids.

This paper investigates a possible implementation of the above idea using carbon nanotubes, because of their unique geometric features (slimness) and thermo-physical properties (high thermal conductivity). Carbon nanotubes (CNTs) have attracted the attention of scientific community, since their mechanical and transport (both electrical and thermal) properties were proven to be superior compared to traditional materials. This observation has motivated intensive theoretical and experimental efforts during the last decade, towards the full understanding/exploitation of these properties [12–16]. Despite these expectations, however, it is reasonable to say that these efforts are far from setting out a comprehensive theoretical framework able to clearly describe these phenomena. First of all, the vast majority of carbon nanotubes (mainly multi-walled) exhibits a metallic behavior but the phonon mechanism (lattice vibrations) of heat transfer is considered the prevalent one close to room temperature [17, 18]. The phonon mean free path, however, is strongly affected by the existence of lattice defects, which is actually a very common phenomenon in nanotubes and closely linked to manufacturing methods. Secondly, there is the important

issue of quantifying the interface thermal resistance between a nanostructure and the surrounding fluid, which affects the heat transfer and the maximum efficiency. Note that, according to the classical theory, there is an extremely low thermal resistance when one reduces the characteristic size of the thermal "antenna" promoting heat transfer [19], as confirmed by numerical investigations for CNTs [20–22]. The present paper investigates, by molecular mechanics based on force fields (MMFF), the thermal performance of nanofins made of single wall CNTs (SW-CNTs). The single wall CNTs were selected mainly due to time constraints of our parallel computational facilities. The following analysis can be split into two parts. First of all, the heat conductivity of SW-CNTs is estimated numerically by both simplified model (Section 1, where this approach is proved to be inadequate) and detailed three-dimensional model (Section 2). This allows one to appreciate the role of model dimensionality (and harmonicity/anharmonicity of interaction potentials) in recovering standard heat conduction (i.e. Fourier's law). This first step is used for validation purposes in a vacuum and for comparison with results from literature. Next, the thermal boundary conductance between SW-CNT and water (for the sake of simplicity) is computed by two methods: the steady state method (Section 3.1), mimicking ideal cooling by strong forced convection (thermostatted surrounding fluid), and transient method (Section 3.2), taking into account only atomistic interactions with the local fluid (defined by the simulation box). This strategy allows one to estimate a reasonable range for the thermal boundary conductance.

1 Heat conductivity of single-wall carbon nanotubes: A simplified model

In order to significantly downgrade the difficulty of studying energy transport processes within a carbon nanotube, Authors often resort to simplified low dimensional systems such as one-dimensional lattices [23–28]. In particular, heat transfer in a lattice is typically modeled by the vibrations of lattice particles interacting with the nearest neighbors and by a coupling with thermostats at different temperatures. The latter are the popular *numerical experiments* based on non-equilibrium molecular dynamics (NEMD). In this respect, to the end of measuring the thermal conductivity of a single wall nanotube (SWNT), we set up a model for solving the equations of motion of the particle chain pictorially reported in Fig. 3 where each particle represents a ring of several atoms in the real nanotube (see also the left-hand side of Fig. 3.2). In the present model, carbon-carbon bonded interactions between *first neighbors* (i.e. atoms of the ith particles and atoms of the particles $i \pm 1$) separated by a distance r are taken into account by a Morse-type potential (shown on the right-hand side of Fig. 3.2) [29] expressed in terms of deviations $x = r - r_0$ from the bond length r_0:

$$V_b\left(x\right) = V_0\left(e^{-2\frac{x}{a}} - 2e^{-\frac{x}{a}}\right), \tag{1}$$

where V_0 is the bond energy while a is assumed $a = r_0/2$. Following [30], bond energy is $V_0 = 4.93[eV]$, while the distance between two consecutive particles at equilibrium is assumed $r_0 = 0.123[nm]$. At any arbitrary configuration the total force, F_i, acting on the ith particle is computed as:

$$F_i = -N_{bon} \sin \vartheta \left[\frac{\partial V_b}{\partial x} (dx_{i-1}) + \frac{\partial V_b}{\partial x} (dx_{i+1}) \right], \tag{2}$$

with $dx_{i-j} = x_i - x_{i-j}$, $dx_{i+j} = x_{i+j} - x_i$ and N_{bon} denoting the number of Carbon-Carbon bonds between two particles, whereas a penalization factor $\sin \vartheta$ may be included to account for bonds not aligned with the tube axis (see Fig. 3.2). Here, we use free-end boundary condition, hence forces experienced by particles at the ends of the chain read:

$$F_1 = -N_{bon} \sin \vartheta \left[\frac{\partial V_b}{\partial x} (dx_2) \right], \quad F_N = -N_{bon} \sin \vartheta \left[\frac{\partial V_b}{\partial x} (dx_{N-1}) \right]. \tag{3}$$

Let p_i and m_i be the momentum and mass of the ith particle, respectively, the equations of motion for inner particles take the form:

$$\frac{dx_i}{dt} = \frac{p_i}{m_i}, \quad \frac{dp_i}{dt} = F_i, \tag{4}$$

whereas the outermost particles $(i = 1, N)$ are coupled to Nosé-Hoover thermostats and are governed by the equations:

$$\frac{dx_i}{dt} = \frac{p_i}{m_i}, \quad \frac{dp_i}{dt} = F_i - \xi p_i, \quad \frac{d\xi}{dt} = \frac{1}{Q} \left[\frac{p_i^2}{2m_i} - N_f k_b T_0 \right], \quad Q = \frac{\tau_T^2 T_i}{4\pi^2}, \tag{5}$$

with k_b, T_0, N_f and τ_T denoting the Boltzmann constant, the thermostat temperature, number of degrees of freedom and relaxation time, respectively, while the auxiliary variable ξ is typically referred to as *friction coefficient* [31]. Nosé-Hoover thermostatting is preferred since it is deterministic and it typically preserves canonical ensemble. However, we notice that (5) represent the equations of motions with a single thermostat. In this case, it is known that the latter scheme may run into ergodicity problems and thus fail to generate a canonical distribution. Although stochastic thermostats (see, e.g., Andersen [32]) are purposely devised to generate a canonical distribution, they are characterized by a less realistic dynamics. Hence, to the end of overcoming the above issues, using deterministic approaches, Martyna *et al.* have introduced the idea of Nosé-Hoover chain [33] (see also [34] and [35] for the equation of motion of Nosé-Hoover chains and further details on thermostats in molecular dynamics simulations). Simulations presented below were carried out using both a single thermostat and a Nosé-Hoover chain (with two thermostats) and no differences were noticed.

Local temperature $T_i(t)$ at a time instant t is computed for each particle i using energy equipartition:

$$T_i(t) = \frac{1}{k_b N_f} \left\langle \frac{p_i(t)^2}{m_i} \right\rangle, \tag{6}$$

where $\langle \rangle$ denotes time averaging. On the other hand, local heat flux J_i transferred between particle i and $i+1$, can be linked to mechanical quantities by the following relationship [25, 27]:

$$J_i = \left\langle \frac{p_i}{m_i} \frac{\partial V_b}{\partial x} (dx_{i+1}) \right\rangle. \tag{7}$$

The above simplified model has been tested in a range of *low* temperature ($300[K] < T < 1000[K]$), where we noticed that it is not suitable to predict normal heat conduction (Fourier's law). In other words, at steady state (i.e. when heat flux is uniform along the chain and constant in time), it is observed a finite heat flux although no meaningful temperature gradient could be established along the chain (see Fig. 2). Thus, the above results predict a divergent heat conductivity. Here, it is worth stressing that one-dimensional lattices with harmonic potentials are known to violate Fourier's law and exhibit a flat temperature profile (and divergent heat conductivity). On one hand, results of the simplified model in Fig. 3 are likely due to a not sufficiently strong anharmonicity. Indeed, as reported on the right-hand side of Fig. 3.2, the Morse function (1) can be safely approximated by an harmonic potential in the range of maximal deviation x observed at low temperature ($T < 1000[K]$), namely $V_b(x) \approx V_0 \left(x^2/a^2 - 1 \right)$. On the other hand, it is worth stressing that it has been demonstrated that anharmonicity alone is insufficient to ensure normal heat conduction [23], in one-dimensional lattice chains.

2 Heat conductivity of single-wall carbon nanotubes: Detailed three dimensional models

In all simulations below, we have adopted the open-source molecular dynamics (MD) simulation package GROningen MAchine for Chemical Simulations (GROMACS) [36–38] in order to investigate the energy transport phenomena in three-dimensional SWNT obtained by a freely available structure generator (Tubegen) [39]. Three harmonic terms are used to describe the carbon-carbon bonded interactions within the SWNT. Namely, a bond stretching potential (between two covalently bonded carbon atoms i and j at a distance r_{ij}):

$$V_b(r_{ij}) = \frac{1}{2} k_{ij}^b \left(r_{ij} - r_{ij}^0 \right)^2, \tag{8}$$

a bending angle potential (between the two pairs of covalently bonded carbon atoms (i,j) and (j,k))

$$V_a(\theta_{ijk}) = \frac{1}{2} k_{ijk}^\theta \left(\cos \theta_{ijk} - \cos \theta_{ijk}^0 \right)^2, \tag{9}$$

and the Ryckaert-Bellemans potential for proper dihedral angles (for carbon atoms i, j, k and l)

$$V_{rb}\left(\phi_{ijkl}\right) = \frac{1}{2}k_{ijkl}^{\phi}\left(1 - \cos 2\phi_{ijkl}\right) \tag{10}$$

are considered in the following MD simulations. Here, θ_{ijk} and ϕ_{ijkl} represent all the possible bending and torsion angles, respectively, while $r_{ij}^0 = 0.142[nm]$ and $\theta_{ijk}^0 = 120°$ are reference geometry parameters for graphene. Non-bonded van der Waals interaction between two individual atoms i and j at a distance r_{ij} can be also included in the model by a Lennard-Jones potential:

$$V_{nb} = 4\epsilon_{CC}\left[\left(\frac{\sigma_{CC}}{r_{ij}}\right)^{12} - \left(\frac{\sigma_{CC}}{r_{ij}}\right)^{6}\right], \tag{11}$$

where the force constants k_{ij}^b, k_{ijk}^θ and k_{ijkl}^ϕ in (8), (9), (10) and parameters (σ_{CC}, ϵ_{CC}) in (11) are chosen according to the table 1 below (see also [40] and [41]). In reversible processes, differentials of heat dQ_{rev} are linked to differentials of a state function, entropy, ds through temperature: $dQ_{rev} = Tds$. Moreover, following Hoover [31, 42], entropy production of a Nosé-Hoover thermostat is proportional to the time average of the friction coefficient $\langle\xi\rangle$ through the Boltzmann constant k_b hence, once a steady state temperature profile is established along the nanotube, the heat flux per unit area within the SWNT can be computed as:

$$q = -\langle\xi\rangle\frac{N_f k_b T}{S_A}, \tag{12}$$

where the cross section S_A is defined as $S_A = 2\pi r b$, with $b = 0.34[nm]$ denoting the van der Waals thickness (see also [43]). Here, the use of formula (12) is particularly convenient since the quantity $\langle\xi\rangle$ can be readily extracted from the output files in GROMACS.

The measure of both the slope of temperature profile along the inner rings of SWNT in Fig. 3 and Fig. 4 and heat flux by (12) enables us to evaluate heat conductivity λ according to Fourier's law. It's worth stressing that, as shown in the latter figures, unlike one-dimensional chains such as the one discussed above, fully three dimensional models do predict normal heat conduction even when using harmonic potentials such as (8), (9) and (10). Nevertheless, we notice that in the above three dimensional model anharmonicity (necessary condition for standard heat conduction in one dimensional lattice chains [23]), despite the potential form itself, intervenes due to a more complicated geometry and the presence of angular and dihedral potentials (9), (10). Interestingly, in our simulations it is possible to drop out at will some of the interaction terms V_b, V_a, V_{rb} and V_{nb} and investigate how temperature profile and thermal conductivity λ are affected. It was found that potentials V_b and V_a are strictly needed to avoid a collapse of the nanotube. Results corresponding to several setups are reported in Fig. 4 and Table 2. It is worth

stressing that, for all simulations in a vacuum, non-bonded interactions V_{nb} proved to have a negligible effect on both the slope of temperature profile and heat flux at steady state. On the contrary, the torsion potential V_{rb} does have impact on the temperature profile while no significant effect on the heat flux was noticed: As a consequence, in the latter case, thermal conductivity shows a significant dependence on V_{rb}. More specifically, the higher torsion rigidity the flatter the temperature profile. Depending on the CNT length (and total number of atoms), computations were carried out for $4\ ns$ up to $6\ ns$ in order to reach a steady state of the above NEMD simulations. Finally, temperature values of the end-points of CNTs (see Figs. 5 and 6) were chosen following others [16], [18].

3 Thermal boundary conductance of a carbon nanofin in water
3.1 Steady state simulations

In this section, we investigate on the heat transfer between a carbon nanotube and a surrounding fluid (water). The latter represents a first step towards a detailed study of a batch of single carbon nanotubes (or small bundles) utilized as *carbon nanofins* to enhance the heat transfer of a surface when transversally attached to it. To this end, and limited by the power of our current computational facilities, we consider a $(5,5)$ SWNT (with a length $L \leq 14[nm]$) placed in a box filled with water (typical setup is shown in Fig. 7). SWNT end temperatures are set at a fixed temperature $T_{hot} = 360[K]$, while the solvent is kept at $T_w = 300[K]$. The carbon-water interaction is taken into account by means of a Lennard-Jones potential between the carbon and oxygen atoms with a parameterization (ϵ_{CO}, σ_{CO}) reported in table 1. Moreover, non-bonded interactions between the water molecules consist of both a Lennard-Jones term between oxygen atoms (with ϵ_{OO}, σ_{OO} from table 3.2) and a Coulomb potential:

$$V_c\left(r_{ij}\right) = \frac{1}{4\pi\varepsilon_0}\frac{q_i q_j}{r_{ij}}, \tag{13}$$

where ε_0 is the permittivity in a vacuum while q_i and q_j are the partial charges with $q_O = -0.82$ e and $q_H = 0.41$ e (see also [41]).

We notice that, the latter is a classical problem of heat transfer (pictorially shown in Fig. 4), where a single fin (heated at the ends) is immersed in a fluid maintained at a fixed temperature. This system can be conveniently treated using a continuous approach under the assumptions of homogeneous material, constant cross section S and one-dimensionality (no temperature gradients within a given cross section) [44]. In this case, both temperature field and heat flux only depend on the spatial coordinate x, and the analytical solution of the energy conservation equation yields, at the steady state, the following

relationship:

$$\tilde{T}(x) = Me^{-mx} + Ne^{mx}, \tag{14}$$

where $\tilde{T}(x) = T(x) - T_w$ denotes the difference between the local temperature at an arbitrary position x and the fixed temperature T_w of a surrounding fluid. Let α and C be the thermal boundary conductance and the perimeter of the fin cross sections, respectively, m is linked to geometry and material properties as follows:

$$m = \sqrt{\frac{\alpha_{st}C}{\lambda S}}, \tag{15}$$

whereas the two parameters M and N are dictated by the boundary conditions, $T(0) = T(L) = T_{hot}$ (or equivalently, due to symmetry, zero flux condition: $dT/dx(L/2) = 0$), namely:

$$M = \tilde{T}(0)\frac{e^{mL/2}}{e^{mL/2} + e^{-mL/2}}, \quad N = \tilde{T}(0)\frac{e^{-mL/2}}{e^{mL/2} + e^{-mL/2}}. \tag{16}$$

Thus, the analytical solution (14) takes a more explicit form:

$$\tilde{T}(x) = \tilde{T}(0)\frac{\cosh[m(L/2 - x)]}{\cosh(mL/2)}, \tag{17}$$

whereas the heat flux at one end of the fin reads:

$$q_0 = m\lambda S\tilde{T}(0)\tanh(mL/2). \tag{18}$$

In the setup illustrated in Fig. 7 and 4, periodic boundary conditions are applied in the x, y and z directions and all simulations are carried out with a fixed time step $dt = 1[fs]$ upon energy minimization. First of all, the whole system is led to thermal equilibrium at $T = 300$ by Nosé-Hoover thermostatting implemented for $0.8[ns]$ with a relaxation time $\tau_T = 0.1[ns]$. Next, the simulation is continued for $15[ns]$ where Nosé-Hoover temperature coupling is applied only at the tips of the nanofin (here, the outermost 16 carbon atom rings at each end) with $T_{hot} = 360[K]$, and water with $T_w = 300[K]$ until, at the steady state, the temperature profile in Fig. 7 is developed. Moreover, pressure is set to $1[bar]$ by Parrinello-Rahman barostat during both thermal equilibration and subsequent non-equilibrium computation. We notice that the above molecular dynamics results are in a good agreement with the continuous model for single fins if $mL/2 = 0.28$. Hence, this enables us to estimate the thermal boundary conductance α_{st} between SWNT and water with the help of eq. (15):

$$\alpha_{st} = \frac{m^2\lambda S}{C}. \tag{19}$$

The thermal conductivity λ has been independently computed by means of the technique illustrated in the sections above for the SWNT alone in a vacuum. Results for a nanofin with $L = 14[nm]$ are reported in

Table 2. We stress that heat flux computed by time averaging of the Nosé-Hoover parameter ξ (see eq. (12)) is also in excellent agreement with the value predicted by the continuous model through eq. (18). For instance, with the above choice $mL/2 = 0.28$, for $(5,5)$ SWNT with $L = 10[nm]$, $L_{NH} = 2[nm]$ in a box $5 \times 5 \times 14[nm^3]$ we have: $-\langle \xi \rangle N_f k_b T = 3.11 \times 10^{-8}[W]$ while

$$q_0 = m\lambda S\tilde{T}(0)\tanh(mL/2) = 3.14 \times 10^{-8}. \tag{20}$$

We stress that L_{NH} is the axial length of the outermost carbon atom rings coupled to a thermostat at each end of a nanotube. Finally, a useful parameter when studying fins is the *thermal efficiency* Ω, expressing the ratio between the exchanged heat flux q and the ideal heat flux q_{id} corresponding to an isothermal fin with $T(x) = T(0)$, $\forall x \in [0, L]$ [44]. In our case, we find highly efficient nanofins:

$$\Omega = \frac{q}{q_{id}} = \frac{m\lambda S\tilde{T}(0)\tanh(mL/2)}{\alpha_{st}C\tilde{T}(0)L/2} = \frac{\tanh(mL/2)}{mL/2} = 0.975. \tag{21}$$

3.2 Transient simulations

The value of thermal boundary conductance between water and a single wall carbon nanotube has been assessed by transient simulations as well. Results by the latter methodology are denoted as α_{tr} in order to distinguish them from the same quantities (α_{st}) in the above section. Here, the nanotube was initially heated to a predetermined temperature T_{hot} while water was kept at $T_w < T_{hot}$ (using in both cases Nosé-Hoover thermostatting for $0.6[ns]$). Next, an NVE molecular dynamics (ensemble where number of particle N, system volume V and energy E are conserved) were performed, where the entire system (SWNT plus water) was allowed to relax without any temperature and pressure coupling. Under the assumption of a uniform temperature field $T_{CNT}(t)$ within the nanotube at any time instant t (i.e. Biot number $Bi < 0.1$), the above phenomenon can be modeled by an exponential decay of the temperature difference $(T_{CNT} - T_w)$ in time, where the time constant τ_d depends on the nanotube heat capacity c_T and the thermal heat conductance α_{tr} at the nanotube-water interface as follows:

$$\tau_d = \frac{c_T}{\alpha_{tr}}. \tag{22}$$

In our computations, following [20], we considered the heat capacity per unit area of an atomic layer of graphite $c_T = 5.6 \times 10^{-4}[Jm^{-2}K^{-1}]$.

The values of τ_d and α_{tr} have been evaluated in different setups, and results are reported in the Table 2. Numerical computations do predict pretty high thermal conductance at the interface (order of 10^7 $[Wm^{-2}K^{-1}]$) with a slight tendency to increase with both the tube length and diameter. It is worth

stressing that values for thermal boundary conductance obtained in this study are consistent with both experimental and numerical results found by others for single wall carbon nanotubes within liquids [20, 45]. However, since the order of magnitude of these results is extremely higher than that involved in macroscopic applications, it may appear as an artifact. Actually it is quite simple to realize that continuum-based models diverge in case of nanometer dimensions, due to the effects of singularity. Hence continuum-based predictions may lead to even higher thermal conductances and they are not even upper bounded, which is clearly unphysical. For example, let us consider the ideal case of a circular cylinder (with diameter D and length L) centered in a square solid of equal length, as reported in Table 3.12 of [19]. The value of thermal boundary conductance can be put into relation with the heat conduction shape factor (CSF) S_f as follows:

$$\alpha_{csf} = \frac{S_f \lambda_w}{\pi D L}, \tag{23}$$

where

$$S_f = \frac{2\pi L}{\ln(1.08w/D)}, \tag{24}$$

and λ_w is the thermal conductivity of the medium, while the square box has dimensions $w \times w \times L$. Let us consider the following example, corresponding to the row "(5, 5), BAD-LJ (sol)" in Table 2 below. Assuming $\lambda_w = 0.58$ $[Wm^{-1}K^{-1}]$, $D = 0.68$ $[nm]$, $w = 4$ $[nm]$, it yields $\alpha_{csf} = 9.2 \times 10^8$ $[Wm^{-2}K^{-1}]$. The analytical results are even larger than those obtained by the steady state simulation (usually larger than those obtained by the transient method). Moreover the continuum-based formula prescribes that thermal conductance (weakly) diverges by reducing the cylinder diameter. On the contrary, molecular dynamics simulations is in line with the expectation of a bounded thermal boundary conductance. In fact, consistently with others [45], we even observe a slight decrease with the tube diameter.

We point out that neither the steady state method nor the transient method fully reproduce the setup described by the analytical formula (23). In fact, in the steady state method all the water bath is thermostatted (while in the analytical formula only the water boundaries are thermostatted) and in the transient method the water temperature changes in time (while the analytical formula is derived under steady state condition). Nevertheless, from the technological point of view, the above results are in line with the basic idea that high aspect-ratio nanostructures (such as carbon nanotubes) are suitable candidates for implementing the above idea of *nanofin*, and thus be utilized for exploiting advantageous heat boundary conductances.

Conclusions

In this work, we first investigate the thermal conductivity of single wall carbon nanotubes by means of classical non-equilibrium molecular dynamics using both simplified one-dimensional and fully three-dimensional models. Next, based on the latter results, we have focused on the boundary conductance and thermal efficiency of single wall carbon nanotubes used as nanofins within water. More specifically, toward the end of computing the boundary conductance α, two different approaches have been implemented. First, $\alpha = \alpha_{st}$ was estimated through a fitting procedure of results by steady state MD simulations and a simple one-dimensional continuous model. Second, cooling of SWNT (at T_{CNT}) within water (at T_w) was accomplished by NVE simulations. In the latter case, the time constant τ_d of the temperature difference ($T_{CNT} - T_w$) dynamics enables to compute $\alpha = \alpha_{tr}$. Numerical computations do predict pretty high thermal conductance at the interface (order of 10^7 [$Wm^{-2}K^{-1}$]), which indeed makes carbon nanotubes ideal candidates for constructing nanofins. We should stress that, consistently with our results $\alpha_{st} > \alpha_{tr}$, it is reasonable to expect that α_{st} represents the upper limit for the thermal boundary conductance, due to the fact that (in steady state simulations) water is forced by the thermostat to the lowest temperature at any time and any position in the computational box. Finally, it is useful to stress that, following the suggestion in [46], all results of this work can be generalized to different fluids using standard nondimensionalization techniques, upon a substitution of the parameterization (ϵ_{CO}, σ_{CO}) representing a different Lennard-Jones interaction between SWNT and fluid molecules.

Methods

The carbon nanotubes geometries simulated in this paper were generated using the program Tubegen [39], while water molecules were introduced using the *SPC/E* model implemented by the *genbox* package available in GROMACS [38]. Numerical results in this work are based on non-equilibrium molecular dynamics where the all-atom forcefields OPLS-AA is adopted for modeling atom interactions. Visualization of simulation trajectories is accomplished using VEGA ZZ [47].

Authors contributions

The engineering motivation for investigating the nanofin idea was provided by P. Asinari. All one-dimensional atomistic simulations and numerical experiments for assessing thermal boundary conductances α were performed by E. Chiavazzo. Measurements of thermal boundary conductance through steady state (α_{st}) and transient simulations (α_{st}) were thought by P. Asinari and E. Chiavazzo respectively.

Computations of thermal conductivity with different combination of interaction potentials, as reported in Fig. 4, were performed by P. Asinari. Authors contributed equally in writing the present manuscript.

Acknowledgments

References

1. Wang L, Fan J: **Nanofluids Research: Key Issues**. *Nanoscale Res Lett* 2010, **5**:1241–1252.

2. Lee K, Yoon S, Jang J: **Carbon Nanofibers: A Novel Nanofiller for Nanofluid Applications**. *Small* 2007, **3**:1209–1213.

3. Hwang Y, Ahn Y, Shin H, Lee C, Kim G, Park H, Lee J: **Investigation on characteristics of thermal conductivity enhancement of nanofluids**. *Current Applied Physics* 2005, **6**:1068–1071.

4. Assael M, Metaxa I, Kakosimos K, Konstantinou D: **Thermal conductivity of nanofluids - Experimental and Theoretical**. *Int. J. Thermophysics* 2006, **27**:999–1017.

5. Terekhov V, Kalinina S, Lemanov V: **The mechanism of heat transfer in nanofluids: State of the art (review). Part 1. Synthesis and properties of nanofluids**. *Thermophysics and Aeromechanics* 2010, **1**:1–14.

6. Bahrami M, Yovanovitch M, Culham J: **Assessment of Relevant Physical Phenomena Controlling Thermal Performance of Nanofluids**. *Journal of Thermophysics and Heat Transfer* 2007, **21**:673–680.

7. Berber S, Kwon YK, Tomanek D: **Unusually High Thermal Conductivity of Carbon Nanotubes**. *Phys. Rev. Lett.* 2000, **84**:4613–4616.

8. Venkata Sastry N, Bhunia A, Sundararajan T, Das S: **Predicting the effective thermal conductivity of carbon nanotube based nanofluids**. *Nanotechnology* 2008, **19**:055704.

9. Acchione T, Fangming D, Fischer J, Winey K: **Thermal Conductivity of Carbon Nanotube/Liquid NanoFluid**. *Proceedings of 2006 APS March Meeting, Baltimore, Maryland* March 2006.

10. Glory J, Bonetti M, Helezen M, Mayne-L'Hermite M, Reynaud C: **Thermal and electrical conductivity of water-based nanofluids prepared with long multi-walled carbon nanotubes**. *Journal of Applied Physics* 2008, **103**:094309.

11. Choi T, Maneshian M, Kang B, Chang W, Han C, Poulikakos D: **Measurement of the thermal conductivity of a water-based single-wall carbon nanotube colloidal suspension with a modified 3-omega method**. *Nanotechnology* 2009, **21**:315706.

12. Berber S, Kwon Y, Tomanek D: **Unusually High Thermal Conductivity of Carbon Nanotubes**. *Phys. Rev. Lett.* 2000, **84**:4613.

13. Kim P, Shi L, Majumdar A, McEuen P: **Thermal Transport Measurements of Individual Multiwalled Nanotubes**. *Phys. Rev. Lett.* 2001, **87**:215502.

14. Donadio D, Galli G: **Thermal Conductivity of Isolated and Interacting Carbon Nanotubes: Comparing Results from Molecular Dynamics and the Boltzmann Transport Equation**. *Phys. Rev. Lett.* 2007, **99**:255502.

15. Alaghemandi M, Algaer E, Böhm M, Müller-Plathe F: **The thermal conductivity and thermal rectification of carbon nanotubes studied using reverse non-equilibrium molecular dynamics simulations**. *Nanotechnology* 2009, **20**:115704.

16. Shelly R, Toprak K, Bayazitoglu Y: **Nose-Hoover thermostat length effect on thermal conductivity of single wall carbon nanotubes**. *Int. J. of Heat and Mass Transfer* 2010, **53**:5884–5887.

17. Dresselhaus M, Eklund P: **Phonons in carbon nanotubes**. *Adv. Phys.* 2000, **49**:705.

18. Zhong H, Lukes J: **Interfacial thermal resistance between carbon nanotubes: Molecular dynamics simulations and analytical thermal modeling**. *Phys. Rev. B* 2006, **74**:125403.

19. Bejan A, Kraus A: *Heat Transfer Handbook*. Hoboken, New Jersey: John Wiley and Sons, Inc. 2003.

20. Huxtable S, *et al*: **Interfacial heat flow in carbon nanotube suspensions**. *Nat. Mater.* 2003, **2**:731–734.

21. Shenogin S, Bodapati A, Xue L, Ozisik R, Keblinski P: **Effect of Chemical Functionalization on Thermal Transport of Carbon Nanotube Composites**. *Appl. Phys. Lett.* 2004, **85**:2229.

22. Stevens R, Zhigilei L, Norris P: **Effects of Temperature and Disorder on Thermal Boundary Conductance at Solid-Solid Interfaces: Nonequilibrium Molecular Dynamics Simulations**. *Int. J. of Heat and Mass Transfer* 2007, **50**:3977–3989.

23. Savin A, Gendelman O: **Heat conduction in one-dimensional lattices with on-site potential**. *Phys. Rev. E* 2003, **67**:041205.

24. Kaburaki H, Machida M: **Thermal conductivity in one-dimensional lattices of Fermi-Pasta-Ulam type**. *Physics Letters A* 1993, **181**:85–90.

25. Liu Z, Li B: **Heat Conduction in simple networks: The effect of interchain coupling**. *Phys. Rev. E* 2007, **76**.

26. Nianbei L: **Effective Phonon Theory of Heat Conduction in 1D Nonlinear Lattice Chains**. *PhD thesis*, National University of Singapore, Department of Physics 2007.

27. Musser D: **On Propagation of Heat in Atomistic Simulations** , Master thesis by University of Akron, 2010.

28. Li B, Wang L: **Thermal logig gates: Computation with phonons**. *Phys. Rev. Lett.* 2007, **99**.

29. Morse P: **Diatomic molecules according to the wave mechanics. II. Vibrational levels**. *Phys. Rev.* 1929, **34**:57–64.

30. Brenner DW, Shenderova OA, Harrison JA, Stuart SJ, Boris N, Sinnott SB: **A second-generation reactive empirical bond order (REBO) potential energy expression for hydrocarbons**. *J. Phys.: Condens. Matter* 2002, **14**:783–802.

31. Hoover WG, Hoover CG: **Links between microscopic and macroscopic fluid mechanics**. *Molecular Physics* 2003, **101**:1559–1573.

32. Andersen H: **Molecular dynamics at constant pressure and/or temperature**. *J. Chem. Phys.* 1980, **72**:2384–2393.

33. Martyna G, Klein M, Tuckerman M: **Nosé-Hoover chains: The canonical ensemble via continuous dynamics**. *J. Chem. Phys.* 1992, **97**:2635–2645.

34. Hünenberger PH: **Thermostat Algorithms for Molecular Dynamics**. *Adv. Polym. Sci.* 2005, **173**:105–149.

35. Frenkel D, Smit B: *Understanding Molecular Simulation from Algorithms to Applications*. Academic Press 2002.

36. Berendsen H, van der Spoel D, van Drunen R: **GROMACS: A message-passing parallel molecular dynamics implementation**. *Comp. Phys. Comm.* 1995, **91**:43–56.

37. Lindahl E, Hess B, van der Spoel D: **Gromacs 3.0: A package for molecular simulation and trajectory analysis**. *J. Mol. Mod.* 2001, **7**:306–317.

38. **GROMACS fast flexible free** [http://www.gromacs.org/].

39. **J. T. Frey and D. J. Doren, University of Delaware, Newark DE, 2005. TubeGen 3.3** [http://turin.nss.udel.edu/research/tubegenonline.html].

40. Guo Y, Karasawa N, Goddard W: **Prediction of fullerene packing in $C_6 0$ and $C_7 0$ crystals**. *Nature* 1991, **351**:464–467.

41. Walther JH, Jaffe R, Halicioglu T, Koumoutsakos P: **Carbon Nanotubes in Water: Structural Characteristics and Energetics**. *J. Phys. Chem. B* 2001, **105**:9980–9987.

42. Hoover WG, Posch HA: **Second-law irreversibility and phase-space dimensionality loss from time-reversible nonequilibrium steady-state Lyapunov spectra**. *Phys. Rev. E* 1994, **49**:1913–1920.

43. Shelly RA, Toprak K, Bayazitoglu Y: **Nose-Hoover thermostat length effect on thermal conductivity of single wall carbon nanotubes**. *Inter. J. Heat and Mass Transfer* 2010, **53**:5884–5887.

44. Kreith F, Bohn MS: *Principles of Heat Transfer*. Brooks/Cole 2001.

45. Shenogin S, Xue L, Ozisik R, Keblinski P, Cahill D: **Role of thermal boundary resistance on the heat flow in carbon-nanotube composites**. *J. App. Phys.* 2004, **95**:8136–8144.

46. Zhong H, Lukes JR: **Interfacial thermal resistance between carbon nanotubes: Molecular dynamics simulations and analytical thermal modeling**. *Phys. Rev. B* 2006, **74**:125403.

47. Pedretti A, Villa L, Vistoli G: **VEGA: A versatile program to convert, handle and visualize molecular structure on windows-based PCs**. *J. Mol. Graph* 2002, **21**:47–49.

Figures and Tables

Figure 1: Color online. Eolic parks represent a macroscopic analogy of the proposed *nanofin* concept: Wind towers are slim enough to avoid disturbing the planetary boundary layer, but high enough to reach the region where wind is stronger. Similarly nanofins do not interfere with the thermal boundary layer, but they allow direct energy transfer between the wall and the bulk fluid, thus acting as thermal bridges. The picture of the wind farm is provided as courtesy of the European Commission, October 2010: *EU Guidance on wind energy development in accordance with the EU nature legislation.*

Figure 2: Color online. Left-hand side: According to the one dimensional model described in section 1, a single particle is formed by several carbon atoms lying on the same plane orthogonal to the CNT axis. Particles are linked by means of several carbon-carbon covalent bonds (not aligned with the CNT axis), with r_0 denoting the spacing between particles at rest. Right-hand side: At low temperature, $T < 1000[K]$, small deviations from the rest position are observed so that the adopted potential (1) can be safely approximated by harmonic Taylor expansion about $x = 0$.

Figure 3: Color online. One-dimensional model: Lattice chain of particles interacting according to a Morse-type potential (1). End-particles are coupled to Nosé-Hoover thermostats at different temperature ($T_{hot} = 320[K]$ and $T_{cold} = 280[K]$). Despite of the anharmonicity of the potential, normal heat conduction (Fourier's law) could not be established. Here, heat flux is computed by eq. (7). However, consistent results are obtained by eq. (12) below which predicts: $\langle \xi_{hot} \rangle k_b T_{hot} = - \langle \xi_{cold} \rangle k_b T_{cold} = 1.11 \times 10^{-7}[W]$.

Figure 4: Color online. Pictorial representation of a single nanofin: End-points are maintained at fixed temperature by Nosé-Hoover thermostats. During numerical experiments for evaluating thermal conductivity, simulations are conducted in a vacuum. On the contrary, thermal boundary conductances are evaluated with the nanofin surrounded by a fluid. The latter set-up can be studied by a one dimensional continuous model, where all fields are assumed to vary only along the x-axis.

Figure 5: Color online. Three-dimensional model: Nosé-Hoover thermostats are coupled to the end atoms of a $(5,5)$ SWNT. Both bonded (8) (9) (10) and nonbonded interactions (11) are considered. In a three-dimensional structure, harmonic bonded potentials do give rise to normal heat conduction. Temperature profiles for two lengths ($5.5[nm]$ and $10[nm]$) are reported.

Figure 6: Color online. Several setups have been tested where some of the interaction potentials (8), (9), (10) and (11) are dropped out. BADLJ: V_b, V_{an}, V_{rb} and V_{nb} are considered. BAD: V_b, V_{an}, V_{rb} are considered. BA: V_b and V_{an} are considered. Bw denotes that V_b is computed with a smaller force constant $k_{ij}^b = 42000[kJmol^{-1}nm^{-2}]$ according to [30].

Figure 7: Color online. A $(5,5)$ SWNT (green) is surrounded by water molecules (blue, red). Nosé-Hoover thermostats with temperature $T_{hot} = 360[K]$ are coupled to the nanotube tips, while water is kept at a fixed temperature $T_w = 300[K]$. After a sufficiently long time (here $15[ns]$), a steady state condition is reached. MD simulation results (in terms of both temperature profile and heat flux) are consistent with a continuous one-dimensional model as described by eq. (17) and (18). Image obtained using VEGA ZZ [47].

Figure 8: Color online. Steady state molecular dynamics (MD) simulations. Dimensionless temperature computed by MD (symbols) versus temperature profile predicted by continuous model (line), eq. (17). Best fitting is achieved by choosing $mL/2 = 0.28$. Case with computational box $2.5 \times 2.5 \times 14[nm^3]$.

Figure 9: Color online. Transient simulations: Temperature evolution as predicted by NVE molecular dynamics. Best fitting of exponential decay of the temperature difference $T_{CNT} - T_w$ is achieved by choosing: $\tau_d = 41[ps]$.

Table 1: Parameters for carbon-carbon, carbon-water and water-water interactions are chosen according to [40] and [41].

Carbon-Carbon interactions	
k_{ij}^b	$47890\ kJmol^{-1}nm^{-2}$
k_{ijk}^θ	$562.2\ kJmol^{-1}$
k_{ijkl}^ϕ	$25.12\ kJmol^{-1}$
ϵ_{CC}	$0.4396\ kJmol^{-1}$
σ_{CC}	3.851 Å
Carbon-Oxygen interactions	
ϵ_{CO}	$0.3126\ kJmol^{-1}$
σ_{CO}	3.19 Å
Oxygen-Oxygen interactions	
ϵ_{OO}	$0.6502\ kJmol^{-1}$
σ_{OO}	3.166 Å
Oxygen-hydrogen interactions	
q_O	-0.82 e
q_H	0.41 e

Table 2: Summary of the results of MD simulations in this work. Single wall nanotubes with chirality $(3,3)$, $(5,5)$ and $(15,0)$ are considered, and several combination of interaction potentials are tested. In the first column, B, A, D and LJ stand for bond stretching, angular, dihedrals and Lennard-Jones potentials, respectively, while Bw denotes bond stretching with a smaller force constant $k_{ij}^b = 42000[kJmol^{-1}K^{-1}]$ according to [30]. Simulations are carried out both in a vacuum (vac) and within water (sol).

Chirality, Case	Box $[nm^3]$	L_{NH} $[nm]$	L $[nm]$	λ $\left[\frac{W}{m\,K}\right]$	α_{st} $\left[\frac{W}{m^2\,K}\right]$	α_{tr} $\left[\frac{W}{m^2\,K}\right]$	τ_d $[ps]$	$mL/2$
$(5,5)$, BAD-LJ (vac)	$12 \times 12 \times 12$	1.5	5.5	67	—	—	—	—
$(5,5)$, BwAD-LJ (vac)	$12 \times 12 \times 12$	1.5	5.5	64	—	—	—	—
$(5,5)$, BAD (vac)	$12 \times 12 \times 12$	1.5	5.5	65	—	—	—	—
$(5,5)$, BA (vac)	$12 \times 12 \times 12$	1.5	5.5	49	—	—	—	—
$(5,5)$, BwA (vac)	$12 \times 12 \times 12$	1.5	5.5	48.9	—	—	—	—
$(5,5)$, BAD-LJ (vac)	$20 \times 20 \times 20$	2	10	96.9	—	—	—	—
$(5,5)$, BAD-LJ (vac)	$105 \times 105 \times 105$	25	25	216.1	—	—	—	—
$(5,5)$, BAD-LJ (sol)	$2.5 \times 2.5 \times 14$	2	10	—	5.18×10^7	—	—	0.28
$(5,5)$, BAD-LJ (sol)	$4 \times 4 \times 14$	2	10	—	5.18×10^7	—	—	0.28
$(5,5)$, BAD-LJ (sol)	$4 \times 4 \times 14$	0	14	—	—	1.70×10^7	33	—
$(5,5)$, BAD-LJ (sol)	$5 \times 5 \times 5$	0	3.7	—	—	1.37×10^7	41	—
$(15,0)$, BAD-LJ (sol)	$5 \times 5 \times 5$	0	4.7	—	—	1.60×10^7	35	—
$(15,0)$, BAD-LJ (sol)	$5 \times 5 \times 5$	0	3.8	—	—	1.43×10^7	39	—
$(3,3)$, BAD-LJ (sol)	$5 \times 5 \times 5$	0	3.7	—	—	8.90×10^6	63	—

Inertial sublayer

Nanofin: Small bundles of CNT

Viscous sublayer

Functionalized wall

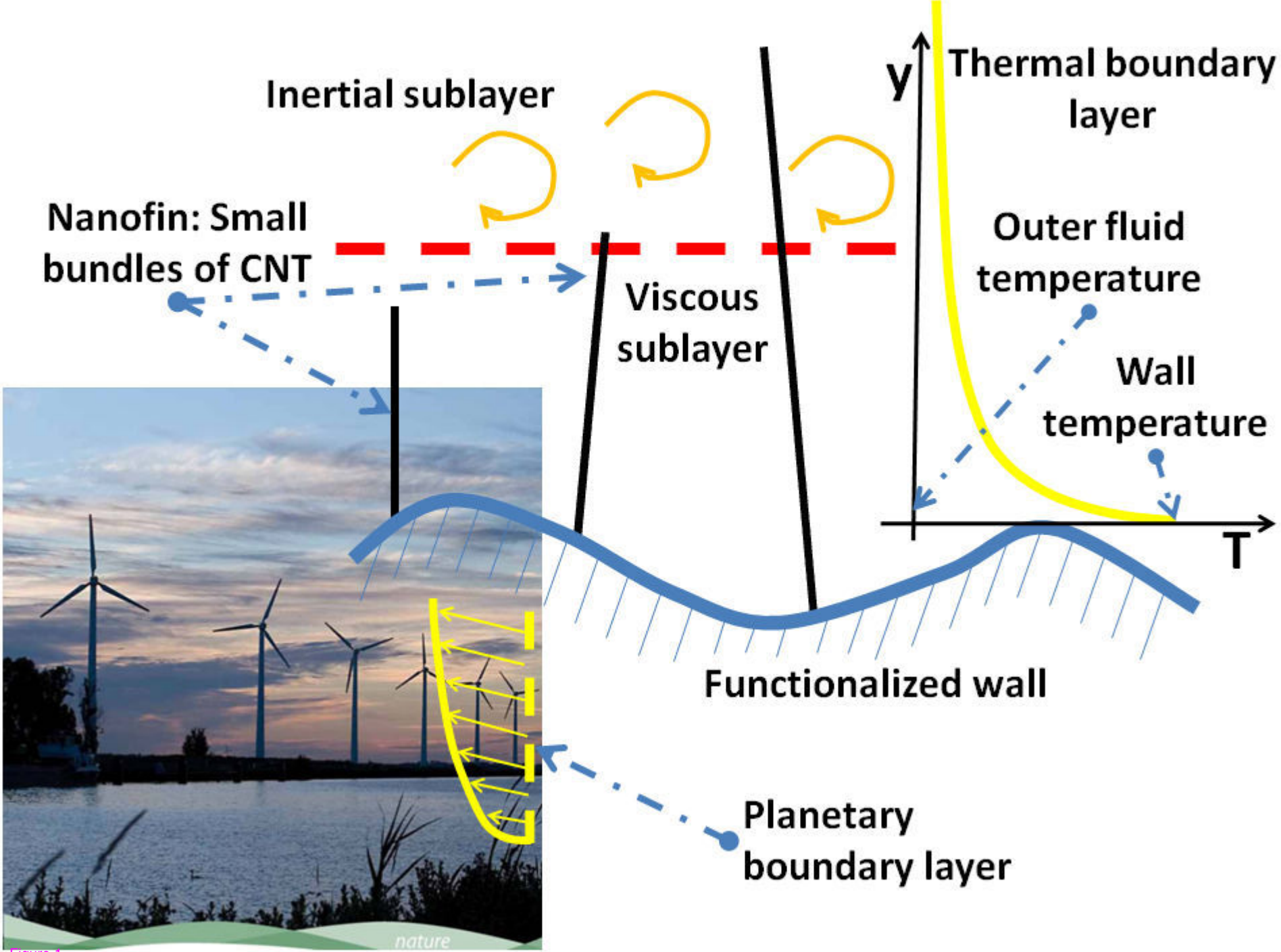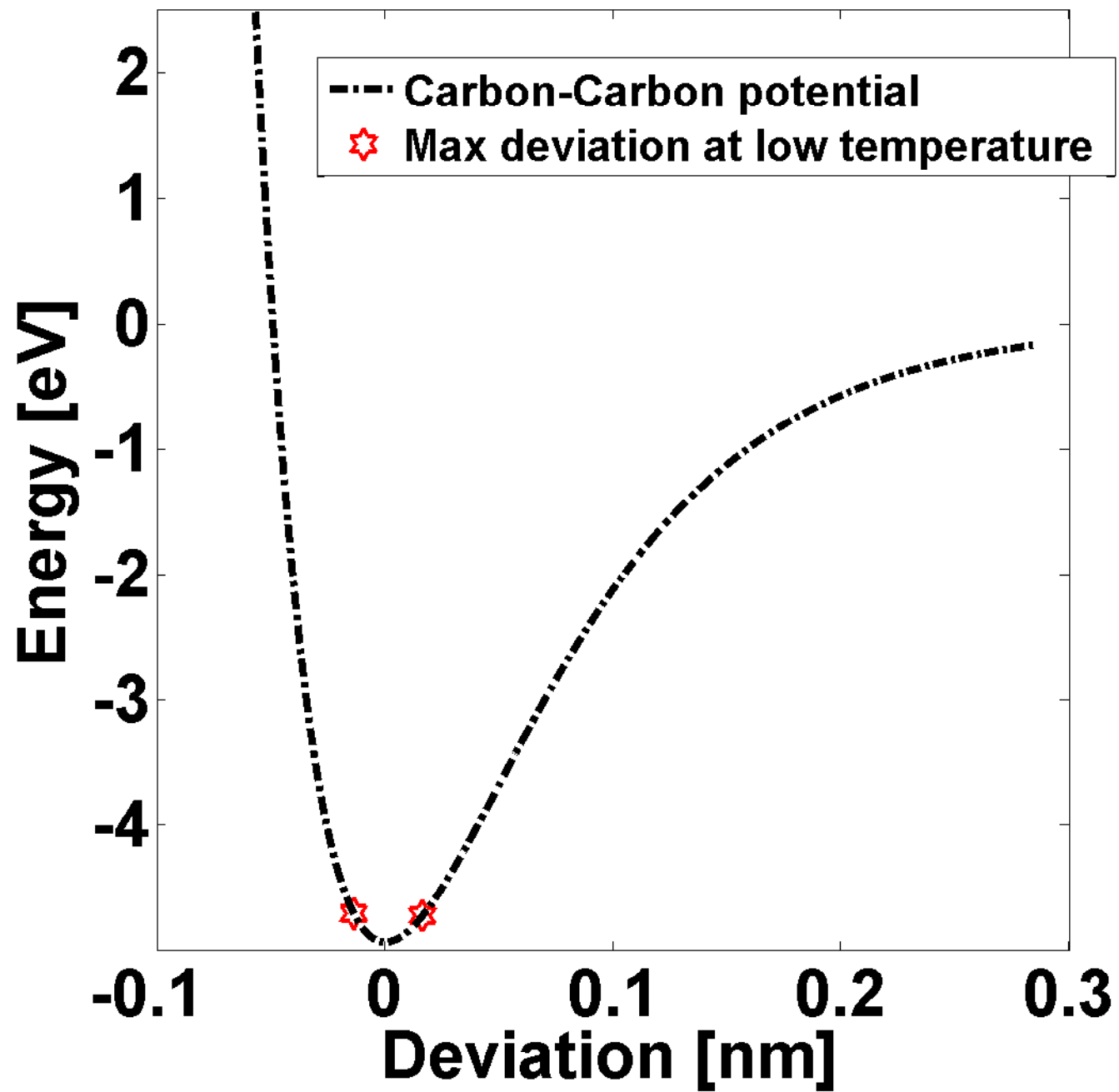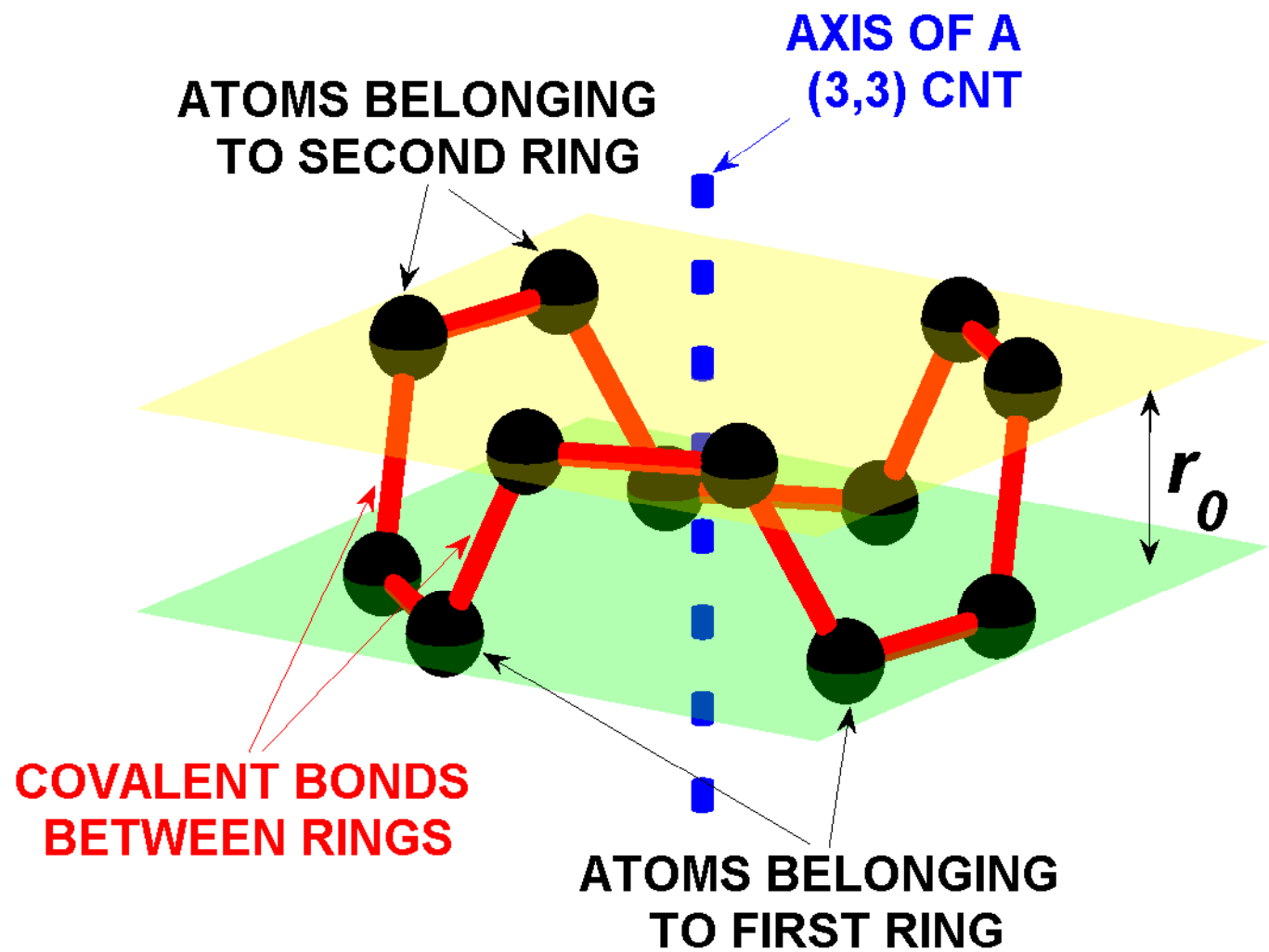Planetary boundary layer

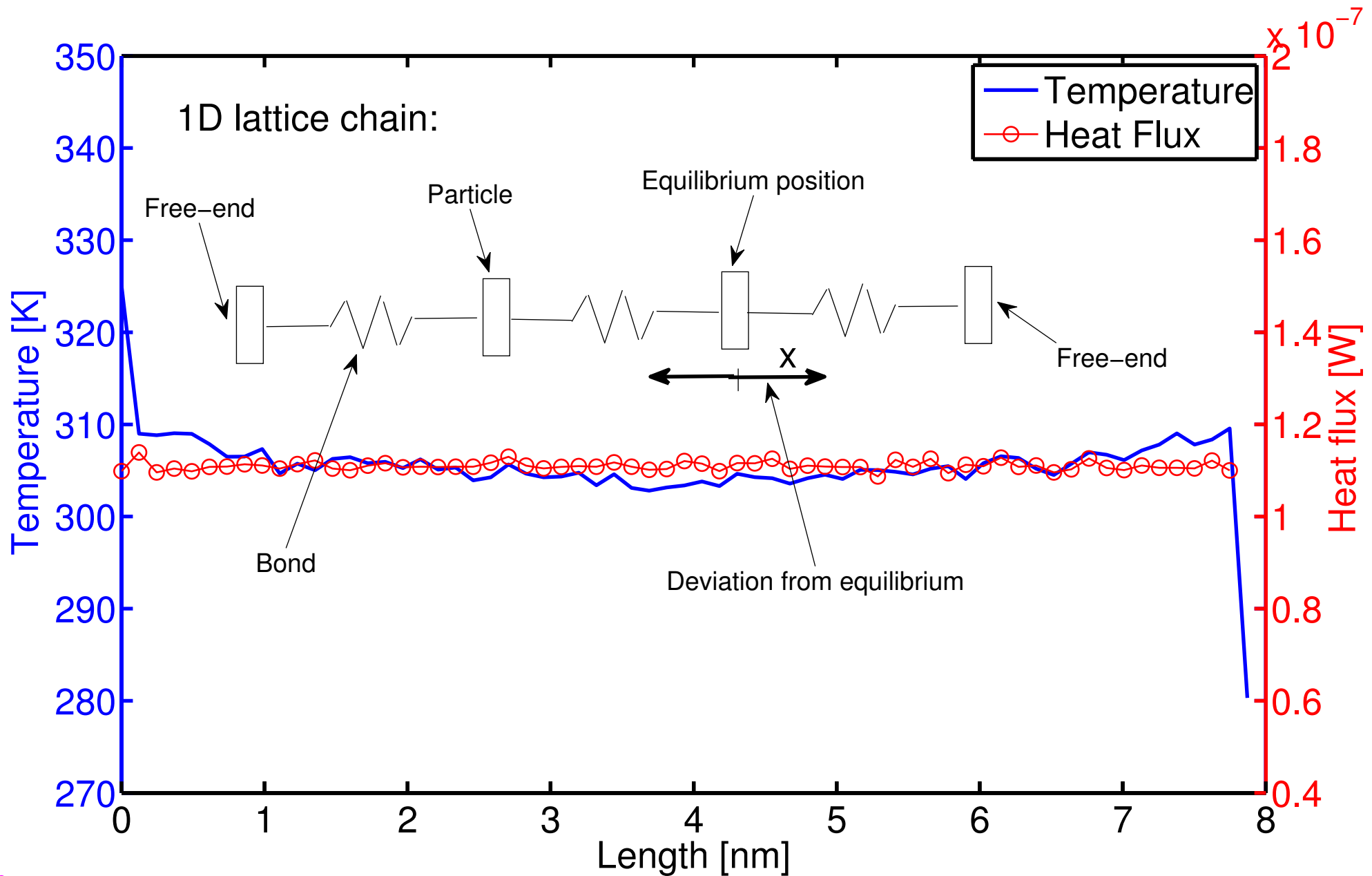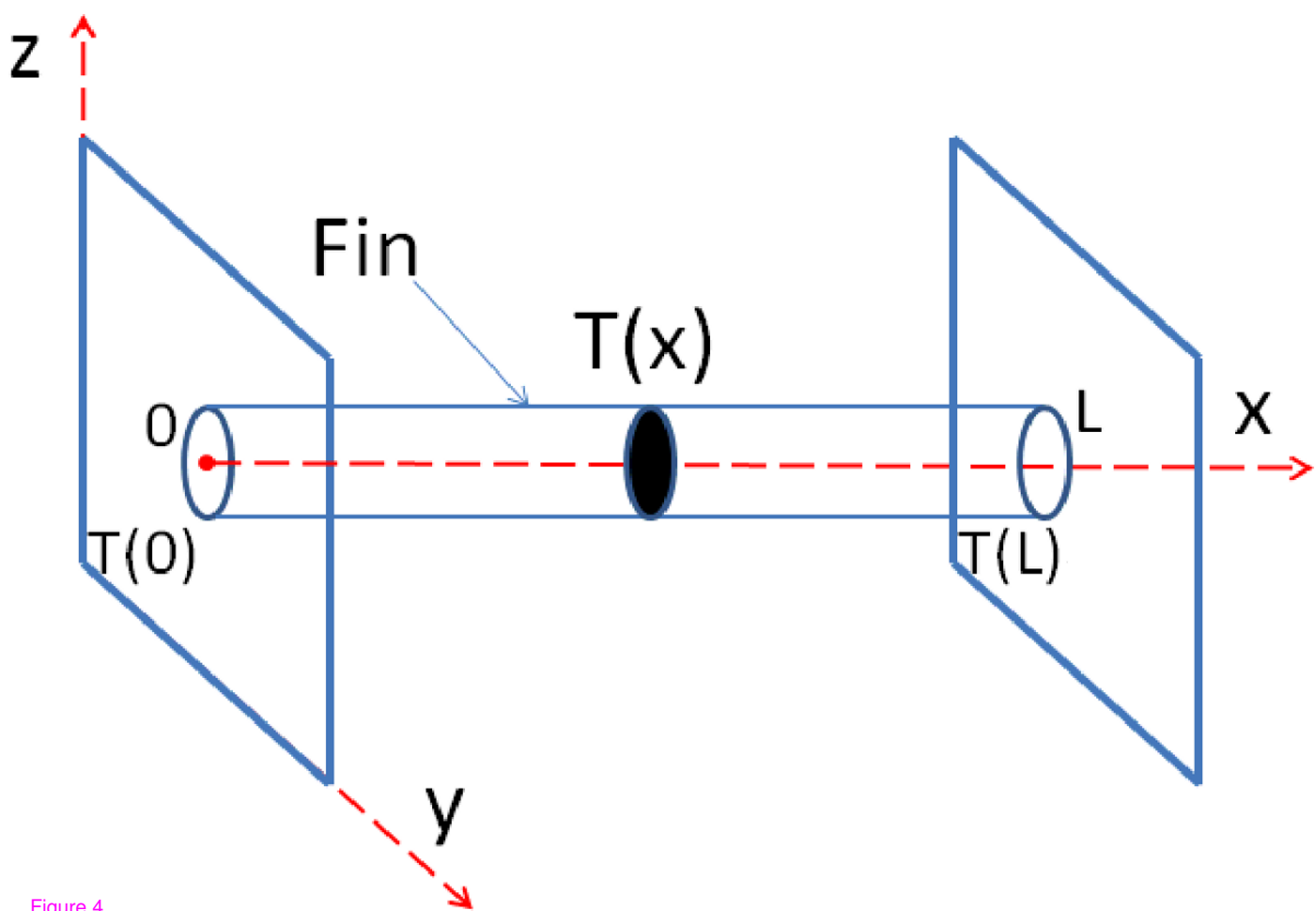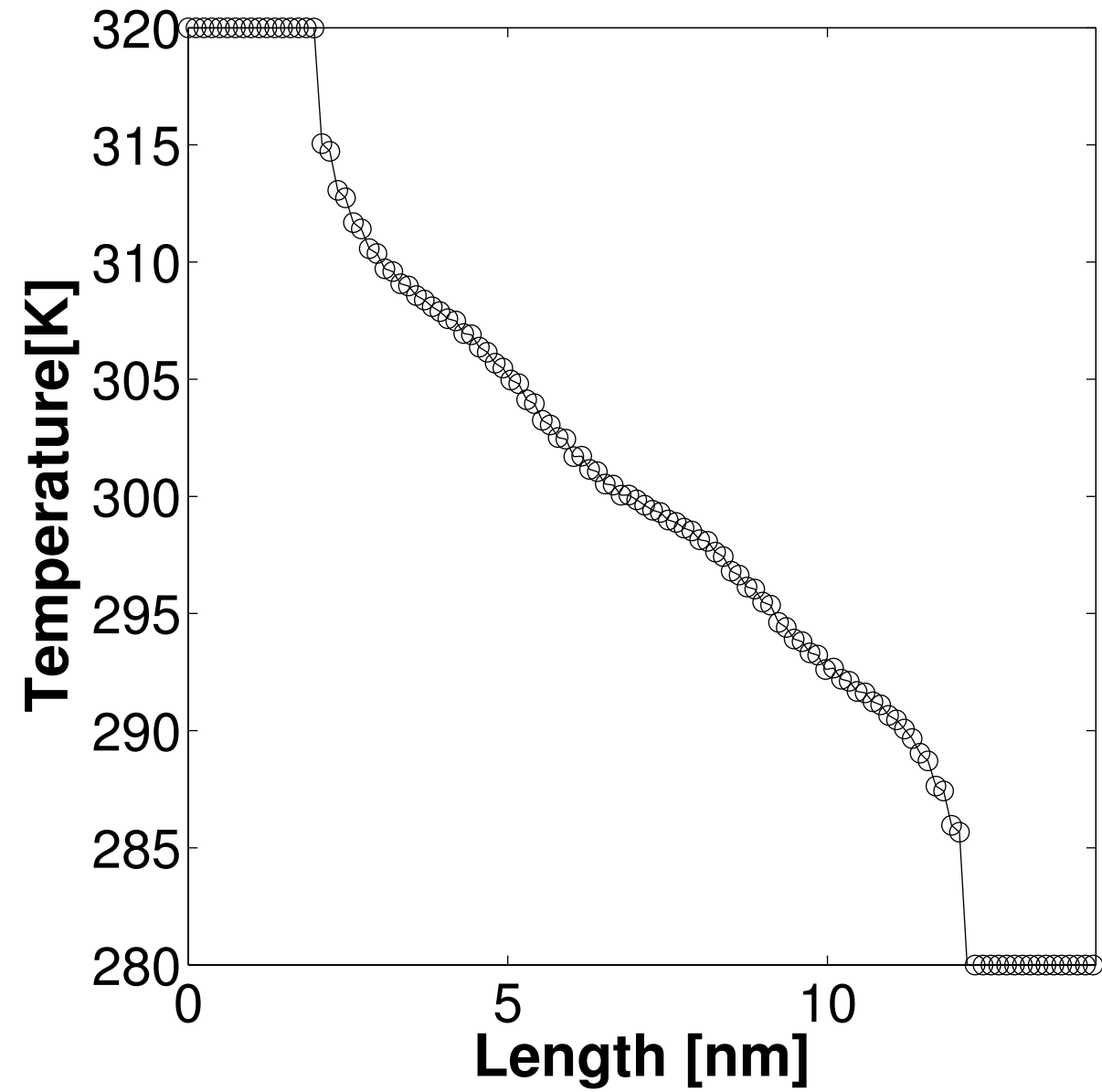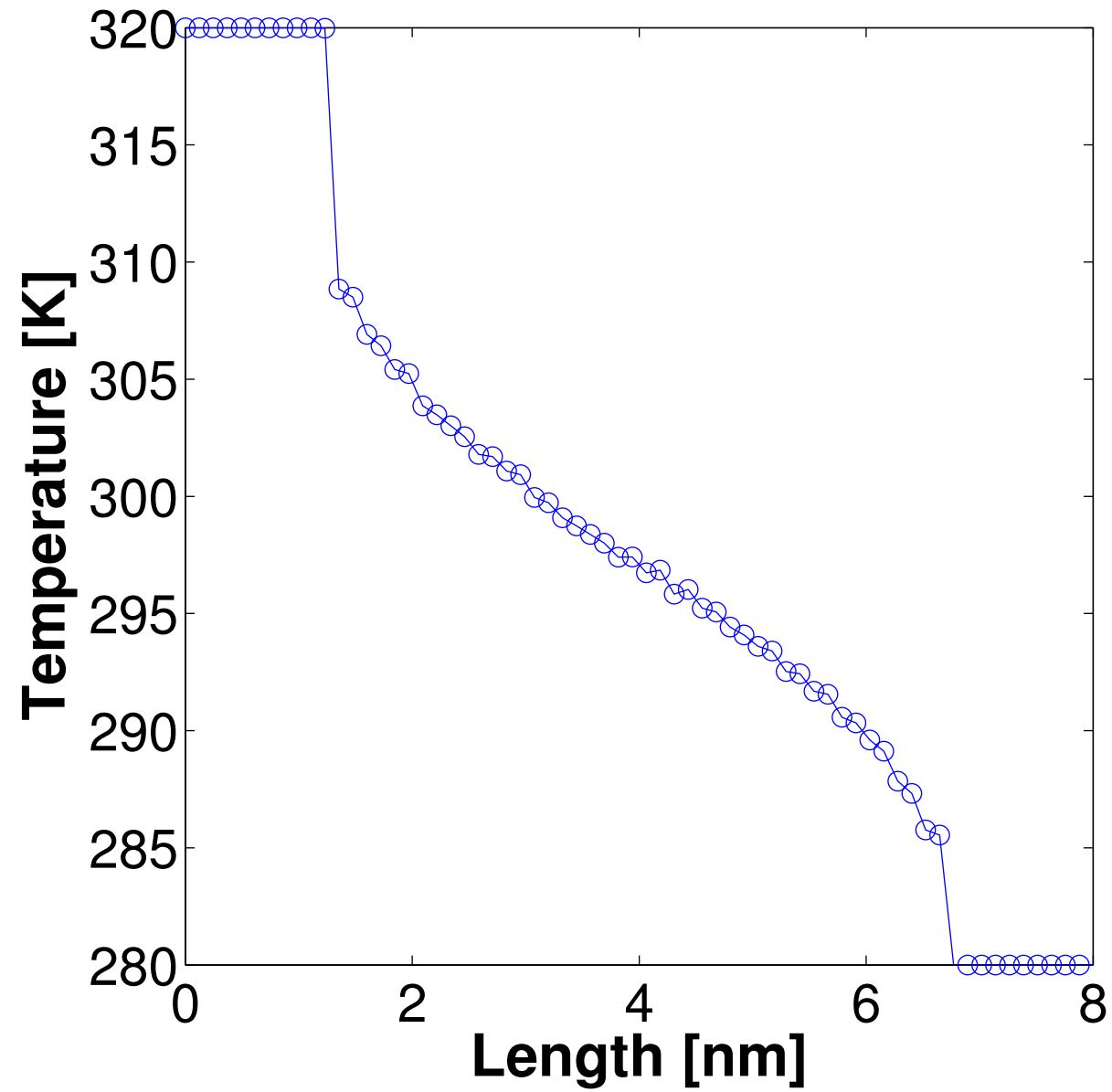Thermal boundary layer

Outer fluid temperature

Wall temperature

y

T

Figure 1

Figure 2

Figure 3

Figure 4

Figure 5
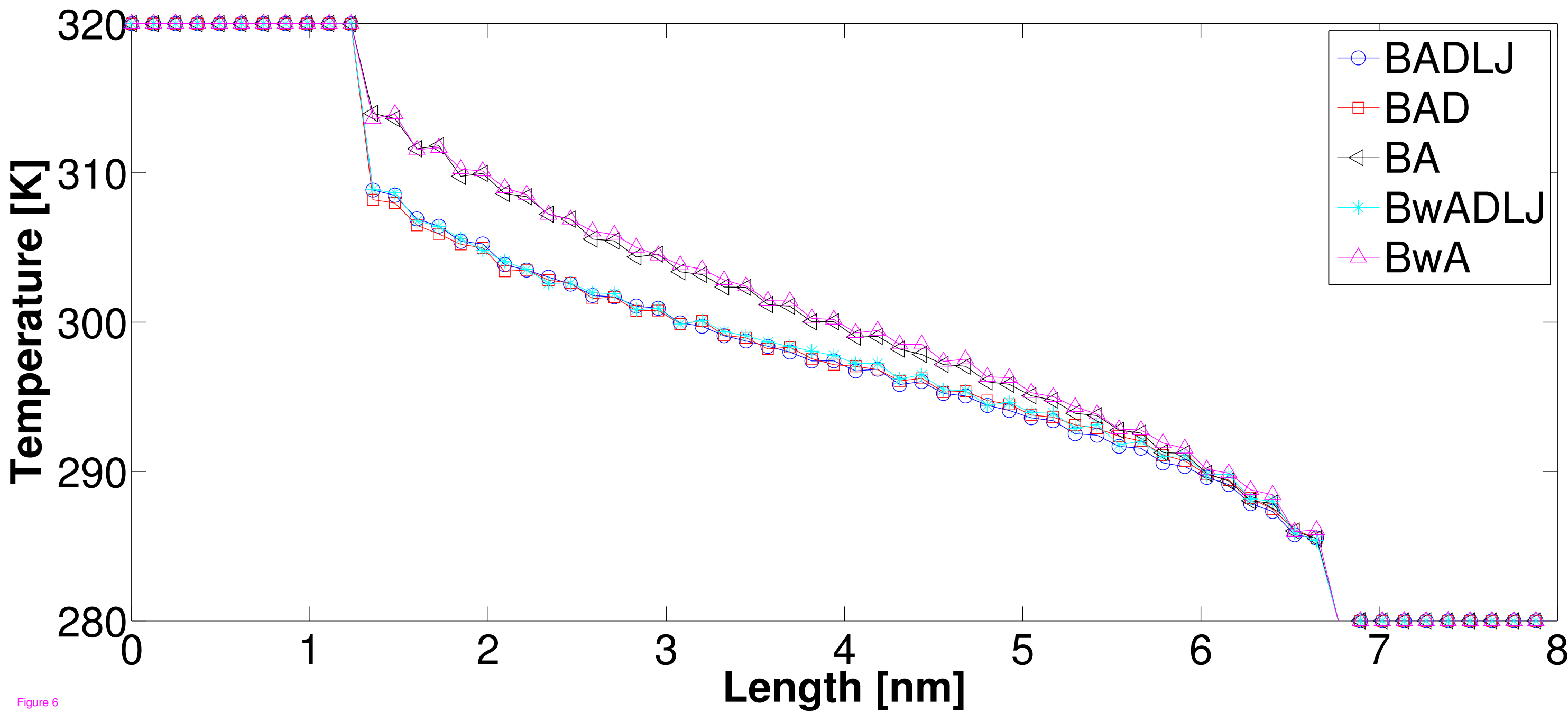
Figure 6
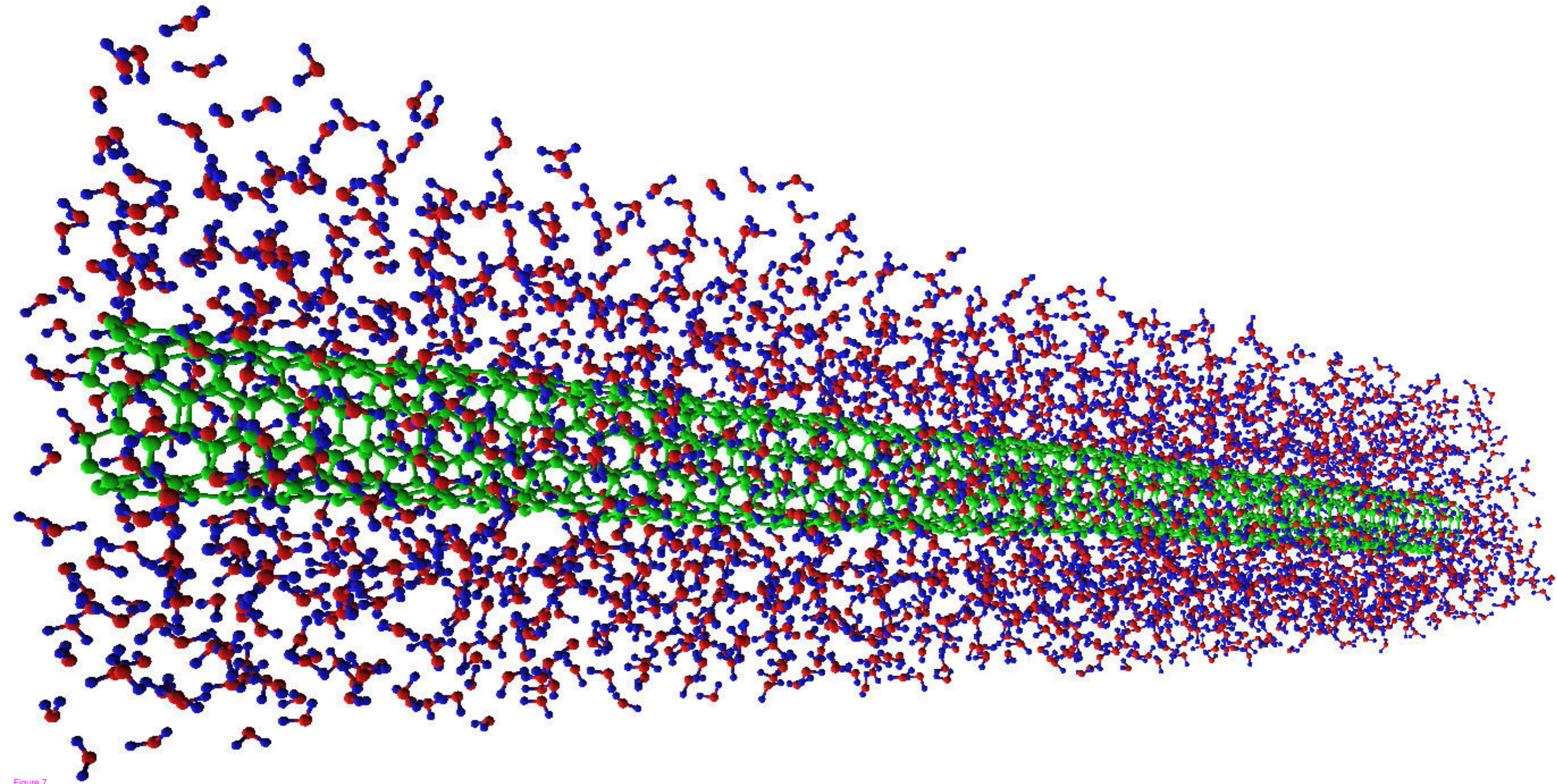
Figure 7
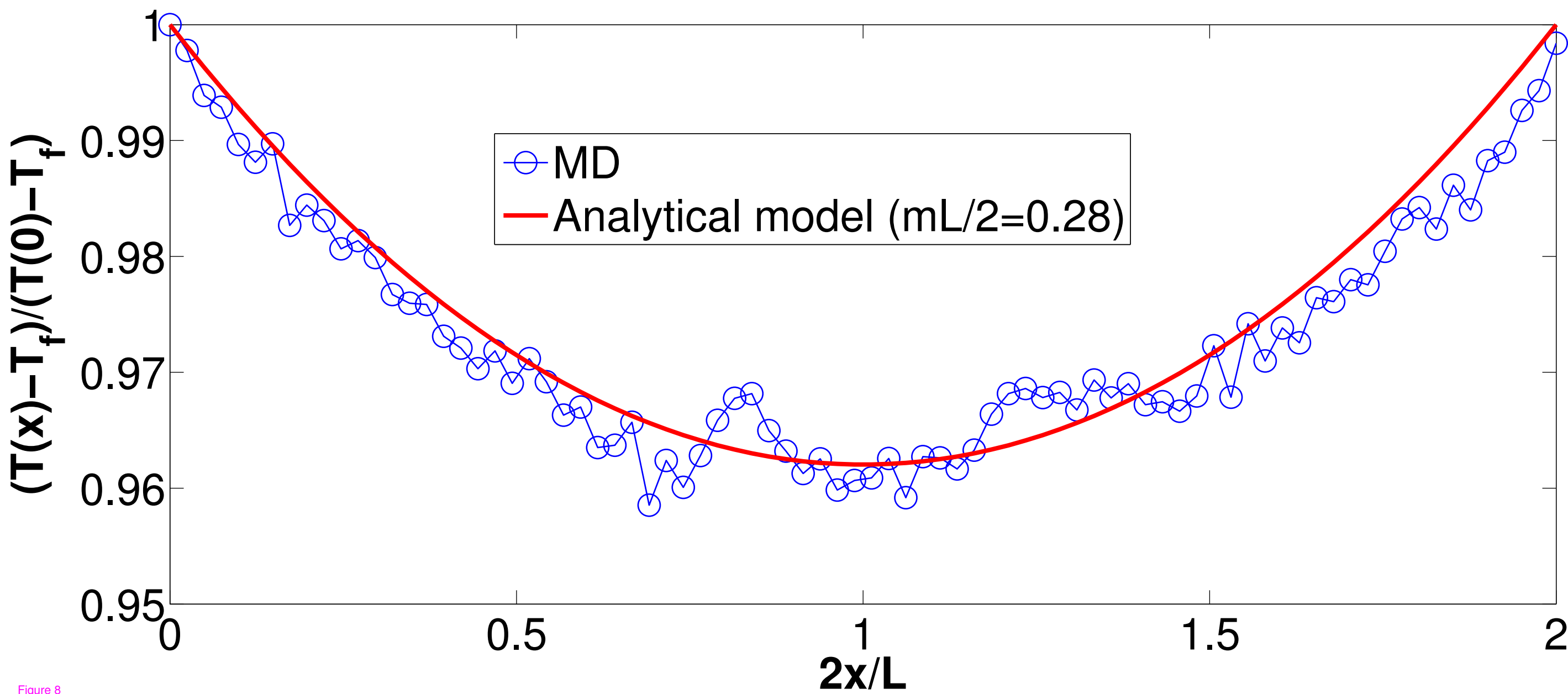
Figure 8

Figure 9
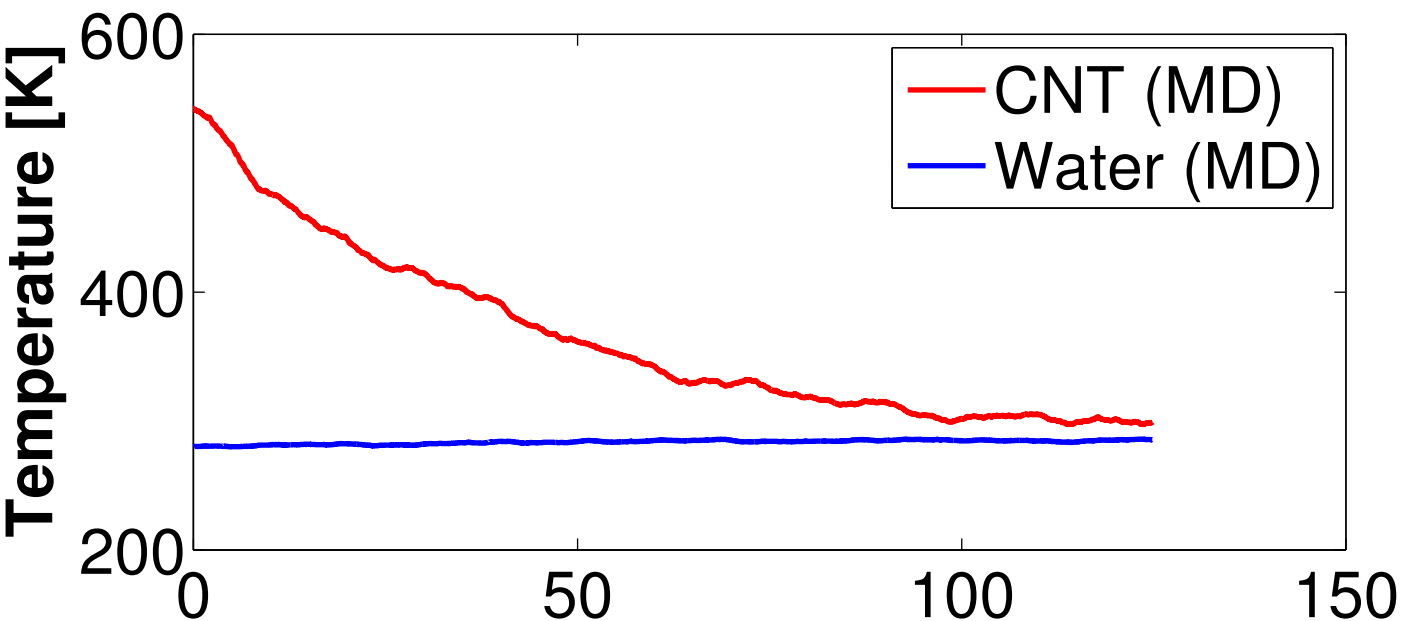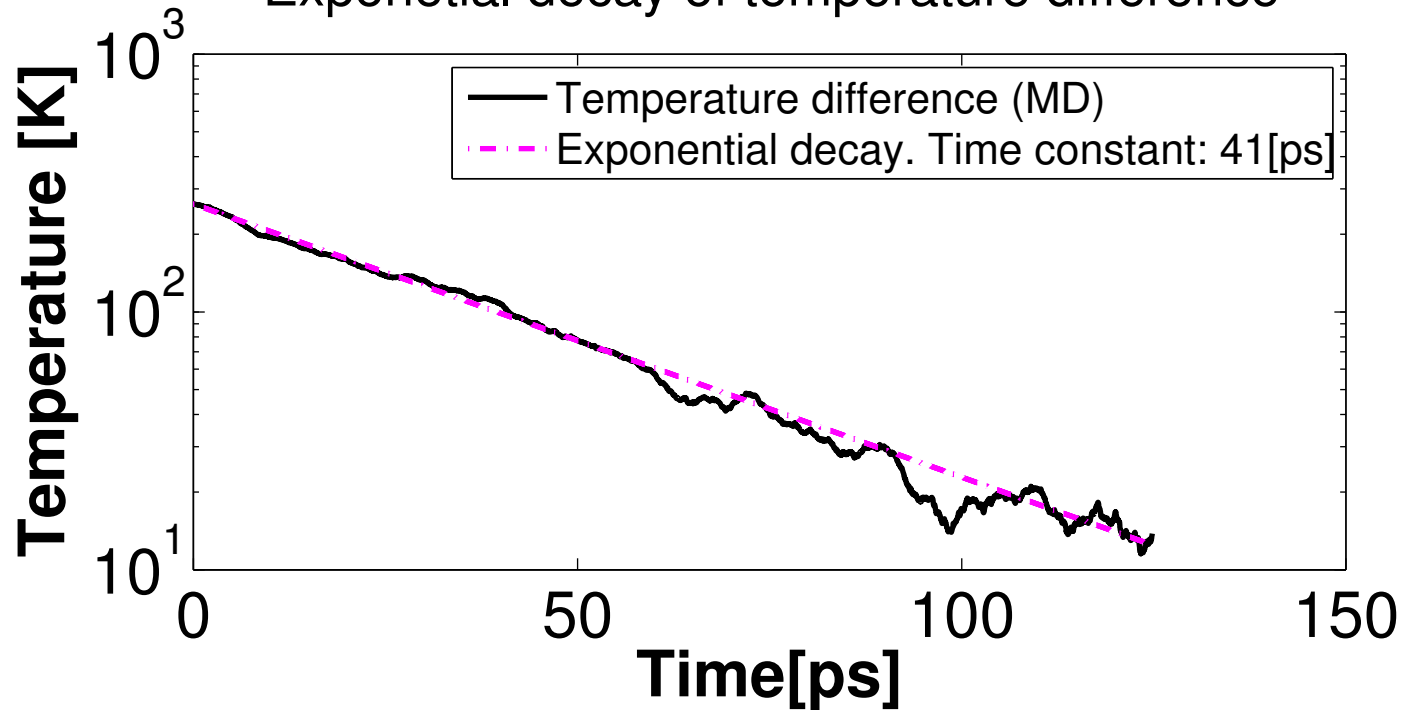
Additional files provided with this submission:

Additional file 1: NANOFIN_Chiavazzo-Asinari_r1.pdf, 436K
http://www.nanoscalereslett.com/imedia/9991513965166817/supp1.pdf
Additional file 2: bmc_article.bib, 20K
http://www.nanoscalereslett.com/imedia/1648920627516682/supp2.bib
Additional file 3: bmc_article.bst, 39K
http://www.nanoscalereslett.com/imedia/1675377151668324/supp3.bst